Crowding-induced Organization of Cytoskeletal Elements: I. Spontaneous Demixing of Cytosolic Proteins and Model Filaments to Form Filament Bundles

Thomas L. Madden and Judith Herzfeld
Department of Chemistry, Brandeis University, Waltham, Massachusetts 02254-9110 USA

ABSTRACT The theory for the effects of crowding on the behavior of reversibly self-assembling solutes is extended to mixtures containing nonassembling solutes. The theory predicts that excluded volume will cause dramatic demixing into domains of long, tightly packed, highly aligned fibers coexisting with an isotropic solution of unaggregated species. It suggests that the bundling of fibers in cells is entropically driven and that accessory binding proteins in the cytoplasm serve to modulate the process rather than create it.

INTRODUCTION

The cytoplasm, which generally contains 20–30% protein by weight, is far more crowded than solutions normally studied in the laboratory (Fulton, 1982; Darnell et al., 1986). In taking the nonideality of such crowded solutions into account, it is usual to assume that the behavior is qualitatively similar to that in dilute solution and that it suffices to make simple quantitative adjustments via activity coefficients. This approach fails in at least two respects. The first, which is common to all crowded solutions, is the occurrence of symmetry breaking. Under crowded conditions, elongated particles will spontaneously align because the translational freedom gained thereby is greater than the rotational freedom lost (Onsager, 1949). At still higher concentrations, positional ordering will occur (even for spherical particles) when the translational entropy lost in the ordered dimension is more than compensated by the translational entropy gained in the other dimensions (Taylor et al., 1989c). These symmetry breaking transitions are usually first order and therefore may occasion separation of the solution into phases with different compositions and ordering. The second difficulty in the use of activity coefficients is peculiar to systems involving self-assembly. On the one hand, the extent of self-assembly depends on the activities of the participating species. On the other hand, the extent of self-assembly affects the activities of all species in solution. As a result, a simple mass action description does not suffice.

Herzfeld et al. have shown that the experimentally observed behavior of crowded self-assembling systems represents a balance between free energy contributions due to monomer interactions at contacts within the aggregates (driving aggregate growth), the ideal entropy of mixing (tending to broaden aggregate size and orientation distributions), excluded volume (driving orientational and positional ordering), and soft repulsions (opposing alignment). For chromonics (polyaromatic dyes and drugs) that stack to form rod-like aggregates, the theory reproduces the experimentally observed sequences of isotropic, nematic, and columnar phases, including the triple point where all three coexist (Taylor and Herzfeld, 1990a, 1990b, 1991). Predictions of average aggregation numbers are also in agreement with estimates made from experimental data (Taylor and Herzfeld, 1991; Boden et al., 1986). For rigid surfactants that assemble into plate-like aggregates, the theory reproduces the experimentally observed sequences of isotropic, nematic, and lamellar phases, including the triple point where they all coexist (Taylor and Herzfeld, 1991). Predictions of average aggregation numbers from this study are also in agreement with experimental results of Boden et al. (Taylor and Herzfeld, 1991; Boden et al., 1987). For ordinary surfactants, capable of forming both rod-like and plate-like micelles, the theory reproduces the experimentally observed rearrangement from aligned rod-like micelles to aligned plate-like micelles with increasing concentration (Taylor et al., 1989a; 1989b). For sickle-cell hemoglobin, a reversibly "polymerizing" protein, the theory reproduces the features of the experimental osmotic pressure curves, including the apparent multicritical point in the isotropic-nematic transition (Hentschke and Herzfeld, 1990, 1991; Herzfeld and Taylor, 1988).

Having successfully described crowded binary systems, we are now in a position to extend the theory to ternary systems, to begin to address the more complex phenomena that can occur in mixtures of proteins. In this first paper of a series, we consider a system consisting of a linearly aggregating species and a second nonaggregating species. This is meant to describe the situation of a model cytoskeletal protein mixed with a soluble protein. The study specifically extends the binary model of Taylor and Herzfeld (1990b). Preliminary results have been presented elsewhere (Madden and Herzfeld, 1992).

METHODS

In this study we model the filaments as spherocylinders, formed by self-assembly of spherical monomers (as shown in Fig. 1). For mathematical simplicity we consider linear

Received for publication 12 April 1993 and in final form 4 June 1993.

0006-3495/93/09/1147/08 $2.00

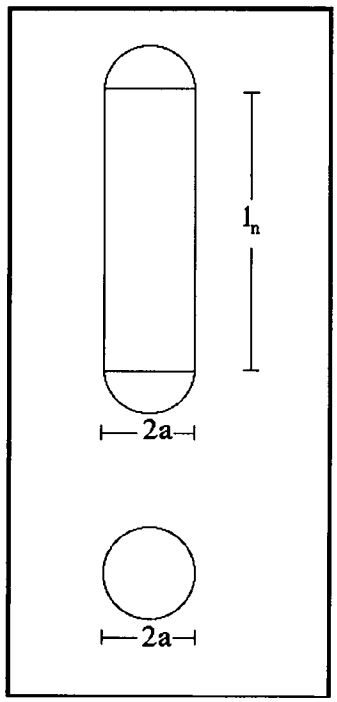

FIGURE 1 Geometries of the particles. In this system n spherical monomers (each of radius a) self-assemble into a spherocylinder of the same total volume, with radius a and cylinder length $l_n = \frac{4}{3}(n - 1)a$.

assembly in which the filaments are one monomer wide. Real cytoskeletal filaments are thicker, but our studies with nonlinear polymers show that most of the distinctive features of the binary and ternary phase diagram remain unchanged as the number of monomers in the cross-section of the polymer increases (Madden, T. L., and J. Herzfeld, submitted). The soluble proteins, which are not allowed to bind to the filaments at all, are modeled as spheres. For simplicity we also restrict particle orientations to a discrete set of three mutually orthogonal axes. This approximation has also been shown to have little effect on the predicted phase behavior (Hentschke and Herzfeld, 1989a).

The state of the system can be described by specifying the number concentration c_{ijn} of particles with orientation i (i = 1, 2, or 3), composed of solute species j (j = A or B), with aggregation number n (where $n = 1$ for j = B and $n \geq 1$ for j = A). In the model there are four contributions to the Helmholtz free energy: the free energy of association to form aggregates; the free energy of mixing; the free energy of hard-core excluded volume interactions; and the free energy resulting from soft interparticle repulsions.

$$F = F_{\text{assoc}} + F_{\text{mix}} + F_{\text{hc}} + F_{\text{soft}} \tag{1}$$

Converting to intensive variables, we introduce the free energy density:

$$f = \beta F/V = f_{\text{assoc}} + f_{\text{mix}} + f_{\text{hc}} + f_{\text{soft}} \tag{2}$$

with $\beta = 1/kT$.

The isodesmic assembly of monomers into linear (i.e., single strand) aggregates is described by a phenomenological model that assigns an association free energy of ϕkT to every contact between two monomers, so that

$$f_{\text{assoc}} = -\sum_{ijn} c_{ijn}\phi(n - 1) \tag{3}$$

The free energy of mixing considers aggregates of a given size and orientation as distinct species and has the form:

$$f_{\text{mix}} = \sum_{ijn} c_{ijn}[\ln(c_{ijn}\Lambda_j^3) - 1]. \tag{4}$$

Here the thermal wavelength, Λ_j, is approximated as independent of the size of the particle. This approximation is justified by the small effect that taking the variation of the wavelength into account has on the results (Taylor and Herzfeld, 1990b; 1991).

The interparticle potential between segments of two particles (with both hard-core and soft contributions) is given by

$$U_{12} = \begin{cases} \infty & r_{12} < (a_1 + a_2) \\ JkT\Omega_1 \cdot \Omega_2 & (a_1 + a_2) < r_{12} < (a_1 + a_2 + \zeta) \\ 0 & r_{12} > (a_1 + a_2 + \zeta) \end{cases} \tag{5}$$

where r_{12} is the distance between the segments of particles 1 and 2 and Ω_m is a unit vector describing the orientation of particle m. This potential contains a hard-core of radius a_m for particle m, which is treated with scaled-particle theory, following the method of Cotter and Wacker (1978). The resulting expression for the hard-core free energy is then:

$$f_{\text{hc}} = -c_p \ln(1 - v_p) + \frac{B}{2(1 - v_p)} + \frac{C}{3(1 - v_p)^2} \tag{6}$$

where

$$v_p = \sum_j v_j, \quad \text{with} \quad v_j = \sum_{in} c_{ijn}b_{jn}, \quad \text{and} \quad b_{jn} = \frac{4}{3}\Pi a_j^3 n, \tag{7}$$

is the total particle volume fraction,

$$c_p = \sum_{ijn} c_{ijn} \tag{8}$$

is the total particle number concentration,

$$B = \sum_{ijn}\sum_{i'j'n'} c_{ijn}c_{i'j'n'}a_j a_{j'}\Pi \times \left[4(a_j + a_{j'}) + \frac{4}{3}(2a_j + a_{j'})(n - 1) + \frac{4}{3}(2a_{j'} + a_j)(n' - 1) + \frac{32}{9\Pi}(a_j + a_{j'})(1 - \delta_{ii'})(n - 1)(n' - 1)\right] \tag{9}$$

and $C = DE$ with

$$D = \sum_{ijn} c_{ijn}\left[\frac{4\Pi a_j^2}{3}\right][2n + 1] \tag{10}$$

and

$$E = \sum_{ijn} \sum_{i'j'n'} c_{ijn} c_{i'j'n'} a_j^2 a_{j'}^2 \Pi \left[2 + \frac{4}{3}(n-1) + \frac{4}{3}(n'-1) + \frac{32}{9\Pi}(1-\delta_{ii'})(n-1)(n'-1) \right] \quad (11)$$

The potential (Eq. 5) also includes a soft repulsive term for parallel aggregates that consists of a step function of width ξ and height JkT per unit contact area extending around the cylinder. This soft-interaction is treated in the Bragg-Williams approximation (i.e., under the assumption that the interactions are sufficiently weak that particle positions remain random) (Hentschke and Herzfeld, 1989b). The contribution to the free energy from the soft repulsive term is (Taylor and Herzfeld, 1991):

$$f_{\text{soft}} = 0.5J \sum_i \langle k_i \rangle \lambda_i \quad (12)$$

where $\lambda_i = \frac{2}{3} \Sigma_{nj} a_j (n-1) c_{ijn}$ is the total cylinder length per unit volume parallel to direction i and $\langle k_i \rangle$ is the average number of parallel neighbors overlapping the step potential of a given i-oriented cylindrical segment. $\langle k_i \rangle$ is obtained by interpolation between the dilute regime and the high density limit (Taylor and Herzfeld, 1991).

The free energy density of Eq. 2 is a functional of the aggregate size and orientation distribution, $\{c_{ijn}\}$. In order to obtain the equilibrium distribution we minimize

$$\tilde{f}(\{c_{ijn}\}) = f(\{c_{ijn}\}) - \sum_j \chi_j \nu_j(\{c_{ijn}\}) \quad (13)$$

with respect to $\{c_{ijn}\}$. The Lagrange multiplier χ_j is the difference between the chemical potential of the solute j and the chemical potential of the solvent. From the calculus of variations it follows analytically that the equilibrium distribution function has the form

$$c_{ijn} = C_j P_{ij}^{n-1} \quad (14)$$

where C_j is the concentration of monomers of species j and P_{ij} is the elongation factor for species j in direction i

$$P_{ij} = \frac{c_{ij(n+1)}}{c_{ijn}} \quad (15)$$

and is related to the equilibrium constant for elongation of filaments of type j in direction i by the equation

$$K_{ij} = \frac{c_{ij(n+1)}}{c_{ijn} c_{ij1}} = \frac{P_{ij}}{C_j}. \quad (16)$$

Substituting Eq. 14 into Eq. 13 gives

$$\tilde{f} = f(\{C_j\}, \{P_{ij}\}) - \sum_j \chi_j \nu_j(\{C_j\}, \{P_{ij}\}). \quad (17)$$

The equilibrium state for given solute and solvent chemical potentials is then obtained by numerically minimizing $\tilde{f}$ with respect to the five distribution parameters C_A, C_B, P_{IA}, P_{2A}, and P_{3A} (P_{1B}, P_{2B}, and $P_{3B} = 0$ since B does not aggregate) for given values of χ_A and χ_B. From this solution we obtain the aggregate size and orientation distributions and the volume fractions, ν_A and ν_B, of particles of each species in the solution. To find the transitions from the isotropic state ($P_{1A} = P_{2A} = P_{3A}$) to the nematic state ($P_{1A} > P_{2A} = P_{3A}$), we select a value of χ_B and, while keeping that χ_B constant, repeatedly bisected χ_A between $\chi_A^{\min}$, which results in a nematic phase, and $\chi_A^{\min}$, which results in an isotropic phase until $|\chi_A^{\max} - \chi_A^{\min}| < 10^{-9}$. Through this process of bisection we find the chemical potentials at the phase transition and the compositions of the coexisting isotropic and nematic phases.

RESULTS AND DISCUSSION

Dilute conditions

In the dilute limit, the interactions among particles are negligible and the free energy consists solely of the ideal terms f_{mix} and f_{assoc} (given by Eqs. 3 and 4). Absent the interactions that drive the isotropic-nematic transition, there is only an isotropic phase (P_{ij}, K_{ij} are independent of i). The ideal state can be calculated analytically with the result that the monomer concentrations are $C_j^{\text{ideal}} = \Lambda_j^{-3} \exp(b_j \chi_j)$, the filament elongation factor is $P_A^{\text{ideal}} = \exp(\phi + b_A \chi_A)$, and the equilibrium constant for filament elongation is

$$K_A^{\text{ideal}} = \frac{P_A^{\text{ideal}}}{C_A^{\text{ideal}}} = \Lambda_A^3 e^{\phi}, \quad (18)$$

independent of χ_A and χ_B. Thus the association free energy, energy ϕkT, and the thermal wavelength Λ_A, can be found from the (in principle) experimentally accessible concentrations of monomers and aggregates in the dilute limit.

Crowded conditions

Fig. 2 shows the effects of nonideality for $\phi = 21$, $J = 1.0$, and $\zeta = 0.10$, when the width of particle A equals the width of particle B. Fig. 2 *a* is a representation of the isotropic-nematic transition line in χ space. The transition was found via serial bisection, as described above. The solid line delineates the value of χ_A at the isotropic-nematic transition for varying values of χ_B. We note that χ_A is insensitive to χ_B for $\chi_B < -18$. The sensitivity of χ_A to χ_B increases rapidly in the range $-18 < \chi_B < -13$ and is constant for $\chi_B > -13$. The dashed lines show osmotic pressure (Π) contours in units of $kT/(a_A)^3$. The contour in the lower left corner is for very dilute conditions when

$$\Pi_{\text{dilute}}/kT = c_p = \Lambda_A^{-3} \exp(b_A \chi_A) + \Lambda_B^{-3} \exp(b_B \chi_B) \quad (19)$$

where in the present case $\Lambda_A = \Lambda_B$ and $b_A = b_B$. At higher solute chemical potentials the osmotic pressure increases. The asymmetry in the diagram at higher concentrations results from the fact that A aggregates and B doesn't.

In Fig. 2 *b* we present the resulting ternary phase diagram in composition space, with low solute volume fractions at the top of the triangle. As we increase the volume fraction of species A along the binary solvent-solute A axis (i.e., moving

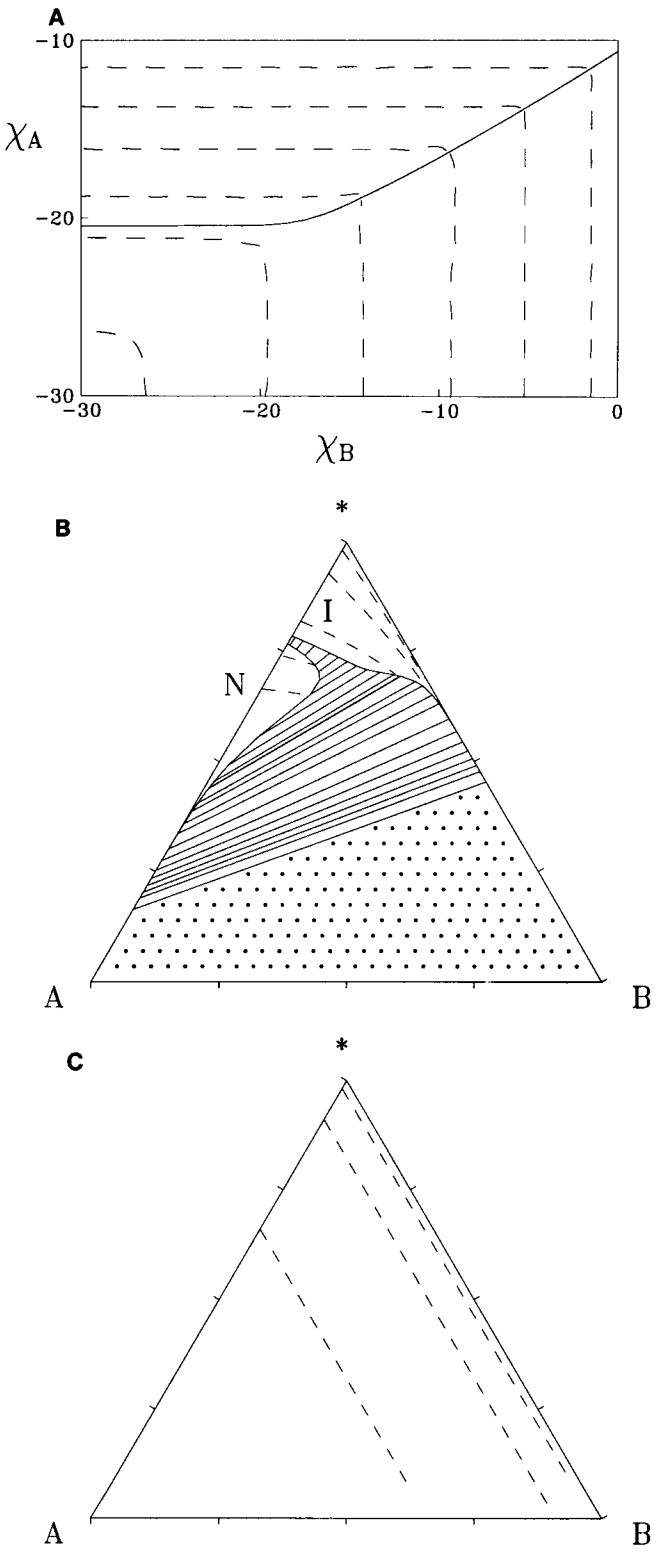

FIGURE 2 (*a*) Representation of the phase behavior in χ space for a free energy of intra-aggregate contacts (in kT) $\phi = 21$, and a step potential height (in $kT/(a_A)^2$) $J = 1.0$ and width (in a_A) $\zeta = 0.10$, when the radii of the solutes are equal. The solid line shows the points at which the state of minimum free energy switches from isotropic (*lower half* of figure) to nematic (*upper half* of figure). The dashed lines show iso-osmotic contours for, starting from the lower left corner, $\Pi = 1.5 \times 10^{-5}$, 0.01, 0.2, 0.6, 1.0, and 1.4 in units of $kT/(a_A)^3$. (*b*) Corresponding ternary composition phase diagram. (*) Solvent. Tie lines connect coexisting isotropic (*I*) and nematic (*N*) phases. The dashed lines in the isotropic phase are contours for constant average aggregation number for solute A, $\langle n_A \rangle$. Starting from the pure solvent apex and moving down $\langle n_A \rangle = 10^{0.25}$, $10^{0.5}$, $10^{0.75}$, $10^{1.0}$, and $10^{1.25}$. The stippled region was numerically intractable. (*c*) Contours for the average aggregation number in the absence of interparticle interactions. Starting from the pure solvent apex and moving down $\langle n_A \rangle = 10^{0.25}$, $10^{0.5}$, and $10^{0.75}$.

down the left leg of the triangle), there is first, at low concentrations of species A, an isotropic phase. Above about 20–25% volume fraction of A, a nematic phase occurs. These results, along the solvent-solute A axis, merely reproduce the results of Taylor and Herzfeld (1990b) for the binary system. For small additional amounts of species B (i.e., moving off the left leg), the position of the phase transition and the width of the two-phase region remain essentially unchanged and we obtain both nematic and isotropic phases accommodating species B. This corresponds to the regime $\chi_B < -18$ in Fig. 2 *a* where χ_A for the isotropic-nematic transition is roughly independent of χ_B. As we increase the amount of solute B, while keeping the ratio of species A to solvent constant (i.e., move along a straight line from the left leg of the diagram toward the "B" corner), the width of the coexistence regime increases until we have a very wide two-phase regime. Here a dense nematic phase that contains very little of species B coexists with a relatively dilute isotropic phase containing comparatively small amounts of species A. The increasing breadth of the two-phase region, with increasing volume fraction of solute, is easily understood in terms of the growing cost in configurational free energy involved in accommodating nonaggregating monomers in the nematic phase as the density of that phase increases. This can be thought of as the difficulty in packing spheres among rods that are roughly parallel: as the density increases, the accommodation decreases. In Fig. 2 *a* this is the regime $\chi_B > -13$; the change of χ_A with χ_B here is greatest. Notice that a line drawn from the right leg to the "A" vertex corresponds to a constant ratio of solvent to B. If solvent and B were to solvate A in the exact same manner, the tie lines in the two phase region would run along such cuts. That the tie lines are more horizontal than these cuts indicates that the ratio of B to solvent is greater in the isotropic than in the nematic phase.

Contours for the average aggregation number for species A

$$\langle n_A \rangle = \left[\sum_{in} n\, c_{iAn} \right] \Big/ \left[\sum_{in} c_{iAn} \right]$$

$$= \left[\sum_{i} (1 - P_{iA})^{-2} \right] \Big/ \left[\sum_{i} (1 - P_{iA})^{-1} \right] \quad (20)$$

are also included in Fig. 2 *b*. The contours in the isotropic phase (where $P_{iA} = P_A$ is independent of i and therefore $\langle n_A \rangle = (1 - P_A)^{-1}$) correspond to $\langle n_A \rangle = 10^{0.25}$, $10^{0.5}$, and $10^{0.75}$. We note that the aggregation of species A, as the amount of solute B in the isotropic phase is increased, occurs at a lower volume ratio of species A to solvent than for the

binary case (constant ratios of species A to solvent are straight lines from the "B" corner to the left leg). This effect is even more pronounced in the nematic phase, where contours for $\langle n_A \rangle = 10^{1.0}$ and $10^{1.25}$ are plotted. This shows the important role that excluded volume plays in the formation of the aggregates.

When interparticle interactions are neglected, the average aggregation number is independent of χ_B. In Fig. 2 *c* we have plotted the corresponding length contours for $\langle n_A \rangle = 10^{0.25}$, $10^{0.5}$, and $10^{0.75}$. (As mentioned above, there is no phase transition under these circumstances.) We see that the aggregation number contours plotted here run parallel to the right leg, meaning that they are at constant volume fractions of species A independent of the concentration of species B. This reflects the fact that in the absence of interparticle interactions solvent (*) and solute B are interchangeable diluents of A. Comparing these results to the more realistic results in Fig. 2 *b*, we see, as expected, that the agreement is closest at low concentrations (near the * vertex). As we follow the $10^{0.25}$ contour from the left-leg of the diagram, we note that, in the more realistic case, it bends toward the right leg. This indicates that the effect of the excluded volume of B is to promote the polymerization of A monomers. Comparisons of the other contours show that the excluded volume of A has a similar effect.

In Fig. 3 we consider stronger aggregation, as is appropriate for cytoskeletal elements. Fig. 3 *a* shows the χ diagram for $\phi = 27$, $J = 1.0$, and $\zeta = 0.10$. We note that, aside from a shift along the axes, Figs. 2 *a* and 3 *a* look very similar. For $\chi_B < -20.0$, χ_A, at the isotropic-nematic transition, is insensitive to χ_B. The sensitivity of χ_A to χ_B increases rapidly in the range $-20 < \chi_B < -15$ to a constant value for $\chi_B > -15$.

In the corresponding composition phase diagram (Fig. 3 *b*) the region of isotropic stability is small compared to Fig. 2 *b*. This result is in agreement with the work of Taylor and Herzfeld (1990b) for the binary system (left-leg) and has a simple explanation. As ϕ is increased the average aggregation length of the polymer of species A, at a given volume fraction, increases. This is apparent from the aggregation number contours that we have plotted in Fig. 3 *b*. Due to the longer polymers, the rotational freedom in the isotropic phase is reduced and the relative advantage of the nematic phase is increased. The width of the isotropic-nematic transition remains narrow for small volume fractions of B. In Fig. 3 *a* this is the regime of $\chi_B < -20.0$ where χ_A is independent of χ_B. For volume fractions of B greater than 20% the transition becomes a great deal wider. Analogous to the case of $\phi = 21$, this can be explained by the tendency of the nematic phase to exclude spherical particles. This wide coexistence regime corresponds to $\chi_B > -15$ in Fig. 3 *a*. Notice that the wide coexistence region can be found at a total solute volume fraction of 25% for $\phi = 27$, whereas for $\phi = 21.0$ the wide regime did not occur until about 35%.

It is also interesting to consider the effect of changing the relative sizes of B and A. Fig. 4 shows results for the case in which the B species has half the width of the aggregating

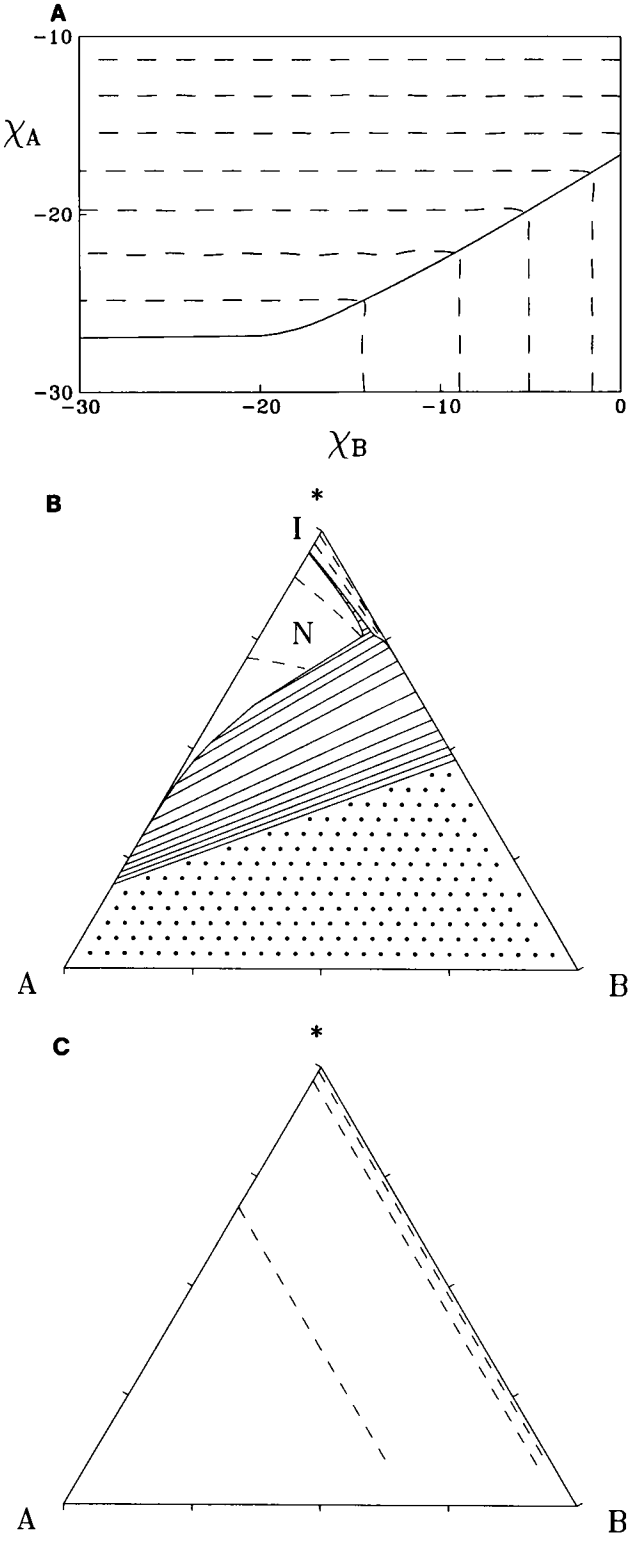

FIGURE 3 As in Fig. 2, except that $\phi = 27$, and the contours represent (*a*) $\Pi = 0.2, 0.6, 1.0, 1.4, 1.8, 2.2$, and 2.6; (*b*) $\langle n_A \rangle = 10^{1.25}, 10^{1.5}, 10^{2.0}$, and $10^{2.5}$, and (*c*) $\langle n_A \rangle = 10^{1.25}, 10^{1.5}$, and $10^{2.0}$.

A species for $\phi = 27$, $J = 1.0$ and $\zeta = 0.10$. We note first that, as necessary, the binary phase behavior, on the left leg of the triangle in Fig. 4, is the same as in Fig. 3 *b*. However, the two-phase region is generally wider in Fig. 4 than in Fig.

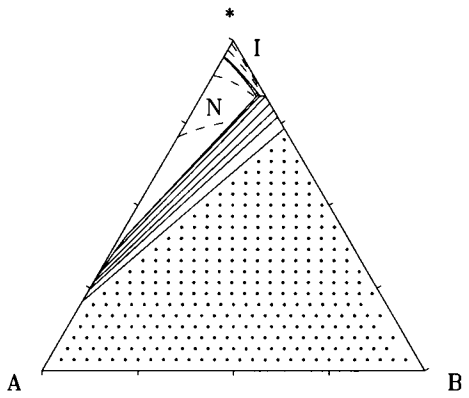

FIGURE 4 As in Fig. 3 *b*, except that the radius of solute B is half that of solute A, $a_A = 2a_B$.

3 *b*. This is understood in terms of the configurational and mixing contributions to the free energy: since the smaller size of B translates to a larger number of particles for a given volume fraction, solvent follows B more strongly to the isotropic phase to maximize the entropy (minimize the free energy) of mixing. It is also worth noting that the tie lines have a slope that is closer to cuts from the right axis to the "A" vertex than in Fig. 3 (such cuts maintain a constant ratio of solvent to B for various values of A). The ratio of B to solvent in the isotropic phase, while still greater than in the coexisting nematic phase, is closer to that of the nematic phase in this diagram than in the previous one. In addition the effects of B on the length of A aggregates is accentuated compared to the previous diagram, due to the greater excluded volume of a given volume fraction of the smaller B particles. Thus in Fig. 4, as B is added, aggregates (of a specific length) are formed at a lower volume fraction of A than in the previous diagram. We see this effect in the $\langle n_A \rangle = 10^{1.25}$ and $10^{1.5}$ contours that are plotted in the isotropic phase as well as in the $\langle n_A \rangle = 10^{2.0}$ contour that is plotted in the nematic phase.

In Fig. 5 we display results for a system that has the same parameters as in Fig. 4, except that the soft repulsions are 50% stronger ($J = 1.5$ rather than 1.0). In the binary system

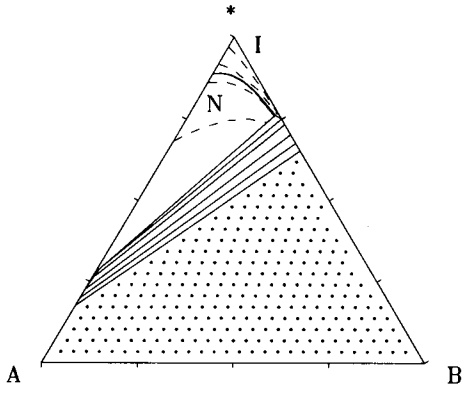

FIGURE 5 As in Fig. 4, except that the soft-repulsions are stronger. Here $J = 1.5$ rather than 1.0.

(left-leg) the isotropic-nematic transition occurs at a greater volume fraction in Fig. 5 than in Fig. 4. This results from the effective torque, opposing alignment, that soft-repulsions introduce (Hentschke and Herzfeld, 1989b; Stroobants et al., 1986). As this effect differentially destabilizes high concentrations, the transition is narrower both on the binary axis and off it. The start of the wide coexistence regime is also delayed to a greater total solute volume fraction, but does still occur. In Fig. 5 we have also plotted contours for $\langle n_A \rangle = 10^{1.25}$, $10^{1.5}$, and $10^{2.0}$. We see that these are similar to the corresponding contours of Fig. 4.

GENERAL DISCUSSION AND CONCLUSIONS

It is interesting to contrast our results with those of Flory and Abe (Flory and Abe, 1978; Abe and Flory, 1978). These workers examine a ternary system consisting of a solvent and two rod-like solute species of the same width. The solutes are not self-assembling; all molecules of a species have the same length. These authors obtain phase diagrams qualitatively similar to those presented here. If the two solute species have different axial ratios, they find a large phase separation. The diagrams they obtain are highly unsymmetrical with respect to the two solute species. Both this lack of symmetry and the phase separation increases with the quotient of the axial ratios. In contrast to the results presented here, Flory and Abe find two different nematic phases and do not find as strong a demixing of solute. We attribute these differences to the asymmetric shape of the second solute in Flory and Abe's work.

The results presented above show that crowding is expected to have dramatic effects on the organization of self-assembled fibers at physiologically relevant concentrations. It is already well known that cytoskeletal fibers will spontaneously align at high concentrations; optical birefringence has been observed in solutions of actin filaments (Kasai et al., 1960; Oosawa and Asakura, 1975; Coppin and Leavis, 1992; Newman et al., 1989; Suzuki et al., 1991) and microtubules (Hitt et al., 1990). In the present work we have shown that packing constraints can also induce fiber bundling: the entropic cost of packing spherical particles with aligned rod-like particles is so great that it exceeds the entropic cost of extreme demixing to form a very concentrated phase of aligned rods, that essentially completely excludes the spherical particles, and a relatively dilute isotropic solution, which is relatively depleted of the fiber-forming solute and relatively enriched in the nonaggregating solute. Let us consider, in particular, the case in which the nonaggregating solute has one-half the diameter of the fiber (Fig. 4). A horizontal line one-quarter of the way down from the apex of the triangle corresponds to a total solute concentration of 25 volume% which is within the range of physiological concentrations. Points on the right half of that line, correspond to solute mixtures with a larger volume fraction of the nonaggregating solute than of the self-assembling solute. Except at the extreme right end of the line, where there is essentially none of the fiber-forming material, the self-assembling material

spontaneously separates into domains of long, tightly packed, highly aligned fibers. This configuration, which is reminiscent of the fiber bundles seen in cells, does not depend on accessory binding proteins as crosslinks or anchors. It suggests that the role of the accessory proteins may be to fine tune and control fiber bundling, by modulating the entropically driven packing that occurs spontaneously in crowded solutions, rather than the more widely accepted role of fighting against the entropically driven dispersion of fibers seen in dilute solutions. Spatial gradients in the concentrations of assembly effectors, such as Ca^{2+}, will also influence the extent and location of demixing.

In obtaining our results, we have had to make a number of simplifying assumptions. In the interests of tractability, the particle orientation distribution has been discretized to three mutually orthogonal axes. We have shown previously that this has minimal effects on the phase behavior (Hentschke and Herzfeld, 1989a). We have also assumed that the self-assembling fibers are rigid. This is a poorer assumption for actin than for tubulin. The more flexible the fiber, the less severe the rod-sphere packing problem, the weaker the demixing, and the looser the packing in the separated fiber phase is expected to be. Efforts are under way to introduce fiber flexibility into the theory. The difficulty has been in adapting models of fiber flexibility to the highly polydisperse populations of fibers seen in self-assembling systems. In the present work we have also restricted our attention to linear self-assembly. Since such assembly is isodesmic it requires only one phenomenological free energy parameter (ϕ). However, the assembly of cytoskeletal fibers is nonlinear and cooperative. We have included these features in a more realistic model for sickle cell hemoglobin and find that they affect the quantitative details of the behavior, but not the qualitative features (Madden T. L., and J. Herzfeld, manuscript in preparation).

Finally we should comment on the soft-repulsions that we have used. For normal hemoglobin near the isoelectric pH (a neutral, soluble, quasispherical protein) it has long been known that the nonideality at high concentrations can be accounted for by excluded volume alone (Ross and Minton, 1977). For self-assembling systems, with aligned fibers, soft-repulsions become more important. We assume that these interactions remain relatively weak and have approximated them by a small square potential of modest range which can be treated in the Bragg-Williams approximation. Potentials of more realistic forms can be modeled as a sum of any number of step potentials, but this does not affect the important features of the phase behavior. The potential can also be made stronger or weaker. Stronger repulsions differentially destabilize high concentrations and cause the two-phase region to become narrower. Thus, as the pH deviates from the isoelectric pH, and the protein accumulates net charge, the phase separation would be expected to become somewhat less dramatic. It should also be noted, however, that the accumulation of net charge on the protein will also weaken self-assembly.

Taking the above considerations into account, we expect our results to be quite robust. Standard statistical mechanics is used to anticipate the behavior of macromolecular solutions under crowded conditions based on macromolecular properties determined under dilute conditions. The effects of packing constraints in crowded self-assembling systems are expected to include spontaneous fiber alignment and dramatic demixing from soluble proteins. Consideration of the role of accessory proteins should take these phenomena into account.

Note added in proof—We have recently learned of experimental observations of crowding-induced filament bundling. Suzuki et al. (1989) found that spontaneous bundling occurred in a solution of 0.5 mg/ml F-actin when ovalbumin was present in excess of 15 wt%. This is in reasonable agreement with Fig. 4, considering that the model parameters were not chosen for the experimental conditions. Poly(ethyleneglycol) induces bundling of F-actin filaments at lower w/w concentrations than ovalbumin (Suzuki et al., 1989; Cuneo et al., 1992) but these results are less readily interpreted because the polymer is less compact than ovalbumin and its specific volume varies with conditions.

The work was supported by National Institutes of Health grant HL-36546 and National Research Service Award HL08472 (to T. L. Madden).

REFERENCES

Abe, A., and P. J. Flory. 1978. Statistical thermodynamics of mixtures of rodlike particles. 2. Ternary mixtures. *Macromolecules.* 11:1122–1126.

Boden, N., R. J. Bushby, C. Hardy, and F. Sixl. 1986. Phase behavior and structure of a non-ionic discoidal amphiphile in water. *Chem. Phys. Lett.* 123:359–364.

Boden, N., R. J. Bushby, K. W. Jolley, M. C. Homes, and F. Sixl. 1987. Factors governing the stability of micellar nematic phases. *Mol. Cryst. Liq. Cryst.* 152:37–55.

Coppin, C. M., and P. C. Leavis. 1992. Quantitation of liquid-crystalline ordering in F-actin solutions. *Biophys. J.* 63:794–807.

Cotter, M. A., and D. C. Wacker. 1978. Van der Waals theory of nematogenic solutions. I. Derivation of the general equations. *Phys. Rev. A.* 18:2669–2675.

Cuneo, P., E. Magri, A. Verzola, and E. Grazi. 1992. "Macromolecular crowding" is a primary factor in the organization of the cytoskeleton. *Biochem J.* 281:507–512.

Darnell, J., H. Lodish, and D. Baltimore. 1986. Molecular Cell Biology. Scientific American Books, New York. 1192 pp.

Flory, P. J., and A. Abe. 1978. Statistical thermodynamics of mixtures of rodlike particles. 1. Theory for polydisperse systems. *Macromolecules.* 11:1119–1122.

Fulton, A. B. 1982. How crowded is the cytoplasm? *Cell.* 30:345–347.

Hentschke, R., M. P. Taylor, and J. Herzfeld. 1989. Equation of state for parallel hard spherocylinders. *Phys. Rev. A.* 40:1678–1680.

Hentschke, R., and J. Herzfeld. 1991. Theory of nematic order with aggregate dehydration for reversibly assembling proteins in concentrated solutions: application to sickle-cell hemoglobin polymers. *Phys. Rev. A.* 43:7019–7030.

Hentschke, R., and J. Herzfeld. 1990. Dehydration of protein polymers in concentrated nematic solutions. *Mat. Res. Soc. Proc.* 177:305–310.

Hentschke, R., and J. Herzfeld. 1989a. Nematic behavior of reversibly polymerizing proteins. *J. Chem. Phys.* 90:5094–5101.

Hentschke, R., and J. Herzfeld. 1989b. Soft repulsions in a lattice model for liquid crystalline order in self-assembling systems. *J. Chem. Phys.* 91: 7308–7309.

Herzfeld, J., and M. P. Taylor. 1988. Unexpected critical points in the nematic behavior of a reversibly polymerizing system. *J. Chem. Phys.* 88:2780–2787.

Hitt, A. L., A. R. Cross, and R. C. Williams. 1990. Microtubule solutions

display nematic liquid crystalline structure. *J. Biol. Chem.* 265:1639–1647.

Kasai, M., H. Kawashima, and F. Oosawa. 1960. Structure of F-actin solutions. *J. Polym. Sci.* 44:51–69.

Madden, T. L., and J. Herzfeld. 1992. Exclusion of spherical particles from the nematic phase of reversibly assembled rod-like particles. *Mat. Res. Soc. Proc.* 248:95–100.

Newman, J., N. Mroczka, and K. L. Schick. 1989. Spontaneous formation of long-range order in actin polymer networks. *Macromolecules.* 22:1006–1008.

Onsager, L. 1949. The effects of shape on the interaction of colloidal particles. *Ann. N. Y. Acad. Sci.* 51:627–660.

Oosawa, F., and S. Asakura. 1975. Thermodynamics of the polymerization of protein. Academic Press, London. 204 pp.

Ross, P. D., and A. P. Minton. 1977. Analysis of non-ideal behavior in concentrated hemoglobin solutions. *J. Mol. Biol.* 112:437–452.

Stroobants, A., H. N. W. Lekkerkerker, and Th. Odijk. 1986. Effect of electrostatic interaction on the liquid crystal phase transition in solutions of rodlike polyelectrolytes. *Macromolecules.* 19:2232–2238.

Suzuki, A., M. Yamazaki, and T. Ito. 1989. Osmoelastic coupling in biological structures: formation of parallel bundles of actin filaments in a crystalline-like structure caused by osmotic stress. *Biochemistry.* 28: 6513–6518.

Suzuki, A., T. Maeda, and T. Ito. 1991. Formation of liquid crystalline phase of actin filament solutions and its dependence on filament length as studied by optical birefringence. *Biophys. J.* 59:25–30.

Taylor, M. P., and J. Herzfeld. 1990a. A model for nematic and columnar ordering in a self-assembling system. *Langmuir.* 6:911–915.

Taylor, M. P., and J. Herzfeld. 1990b. Phase diagram for reversibly-assembled rod-like aggregates: nematic, columnar and crystalline ordering. *Mat. Res. Soc. Proc.* 177:135–140.

Taylor, M. P., and J. Herzfeld. 1991. Shape anisotropy and ordered phases in reversibly assembling lyotropic systems. *Phys. Rev. A.* 43:1892–1905.

Taylor, M. P., A. E. Berger, and J. Herzfeld. 1989a. Theory of amphiphillic liquid crystals: multiple phase transitions in a model micellar system. *J. Chem. Phys.* 91:528–538.

Taylor, M. P., A. E. Berger, and J. Herzfeld. 1989b. A model for nematic phases in a reversibly assembling system of hard rods and plates. *Mat. Res. Soc. Proc.* 134:21–26.

Taylor, M. P., R. Hentschke, and J. Herzfeld. 1989c. Theory of ordered phases in a system of parallel hard spherocylinders. *Phys. Rev. Lett.* 62: 800–803.